Ultrafast Switching of the Electric Polarization and Magnetic Chirality in $BiFeO_3$ by an Electric Field

Satadeep Bhattacharjee,[1*] Dovran Rahmedov,[1] Dawei Wang,[2] Jorge Íñiguez,[3] and L. Bellaiche[1]
[1]Department of Physics and Institute for Nanoscience and Engineering, University of Arkansas Fayetteville, Arkansas 72701, USA
[2]Electronic Materials Research Laboratory, Key Laboratory of the Ministry of Education and International Center for Dielectric Research, Xi'an Jiaotong University, Xi'an 710049, China
[3]Institut de Ciència de Materials de Barcelona (ICMAB-CSIC), Campus UAB, 08193 Bellaterra, Spain
(Received 27 September 2013; revised manuscript received 21 January 2014; published 7 April 2014)

Using a first-principles-based effective Hamiltonian within molecular dynamics simulations, we discover that applying an electric field that is opposite to the initial direction of the polarization results in a switching of both the polarization and the magnetic chirality vector of multiferroic $BiFeO_3$ at an ultrafast pace (namely, of the order of picoseconds). We discuss the origin of such a double ultrafast switching, which is found to involve original intermediate magnetic states and may hold promise for designing various devices.

DOI: 10.1103/PhysRevLett.112.147601 PACS numbers: 77.80.Fm, 75.25.-j, 75.78.Jp, 75.85.+t

The magnetic chirality vector $\boldsymbol{\kappa}$ is proportional to $\mathbf{S}_i \times \mathbf{S}_j$, where $\mathbf{S}_i$ and $\mathbf{S}_j$ are spins of two neighboring sites i and j, respectively. This chirality vector is an important quantity that is related to many interesting phenomena, such as spin-polarized current, spin torque, the anomalous Hall effect, magnetic motors [1–4], etc. It is extensively studied in the context of nanomagnetism [5]. Being able to control and even switch this magnetic chirality vector by the application of an electric field can even further broaden the prospect of designing novel devices, in addition to being of obvious fundamental interest (by, e.g., understanding what governs this hypothetical magnetoelectric coupling). One may also wonder if such hypothetical switching can be ultrafast in nature, and what are the intermediate states involved in this switching (if any).

Here, we explore such possibilities in the multiferroic $BiFeO_3$ (BFO) system. We chose this material because (1) it possesses both a magnetic cycloid (which results in a nonzero $\boldsymbol{\kappa}$) and an electrical polarization at room temperature, and (2) previous studies have demonstrated that applying an electric field in BFO along a direction away from the initial electric polarization leads to a rotation of this polarization and, as a consequence of magnetoelectric effects, to a change in the magnetic cycloidal plane [6–8]. It is thus interesting (and novel) to determine if applying an electric field that is opposite to the initial direction of the polarization can result in an ultrafast switching of both the polarization and the magnetic chirality vector, and how the dipoles and spins rearrange themselves during these possible latter switchings. Via the use of a first-principles-based method, we discover that applying an electric field that is opposite to the initial direction of the polarization does indeed result in an ultrafast (of the order of picoseconds) switching of both the polarization and the magnetic chirality vector. Moreover, these switchings involve striking intermediate states, which makes them promising for applications and fundamentally interesting.

Technically, we use here the first-principles-based effective Hamiltonian method described in Ref. [9] for which the total energy is

$$E_{\text{tot}} = E_{\text{FE-AFD}}(\{\mathbf{u}_i\}, \{\eta_i\}, \{\boldsymbol{\omega}_i\}) + E_{\text{mag}}(\{\mathbf{m}_i\}, \{\mathbf{u}_i\}, \{\eta_i\}, \{\boldsymbol{\omega}_i\}), \quad (1)$$

where $\mathbf{u}_i$ is the local ferroelectric (FE) soft mode in the unit cell i and is directly proportional to the electric dipole of that unit cell. $\{\eta_i\}$ is the strain tensor and contains both homogeneous and inhomogeneous parts. The pseudovectors $\boldsymbol{\omega}_i$ characterize the oxygen octahedra tilts, which are also termed antiferrodistortive (AFD) motions. More precisely, the direction of $\boldsymbol{\omega}_i$ is parallel to the axis about which the oxygen octahedron of the unit cell i rotates, while the magnitude of $\boldsymbol{\omega}_i$ provides the angle of such rotation [10]. $\mathbf{m}_i$ represents the magnetic dipole moment of the Fe ion located inside the unit cell i and has a fixed magnetic moment of $4\mu_B$—as consistent with first principles [11]. The first term in the total energy ($E_{\text{FE-AFD}}$) gathers the energies associated with the structural degrees of freedom of the effective Hamiltonian (electric dipoles, strains, oxygen octahedra tilts) and their mutual interactions. It is described in Refs. [10,12]. The second term (E_{mag}) is given in Ref. [9]. It gathers the magnetic degrees of freedom, their mutual interactions, and their couplings to the lattice degrees of freedom. Technically, it contains long-range magnetic dipolar interactions involving all Fe sites, short-range (up to third-nearest neighbors) direct exchange interaction, and magnetic exchange interaction mediated via the local modes, antiferrodistortive motions, and the strains [13]. It also possesses an energy that involves

oxygen octahedra tiltings and that yields a spin canting [14], as well as another energetic term that is derived from the spin-current model [15,16]. This latter has the analytical form

$$E_{\text{spin-current}} = -C(\mathbf{u}_i \times \mathbf{e}_{ij}) \cdot (\mathbf{m}_i \times \mathbf{m}_j), \tag{2}$$

where $\mathbf{e}_{ij}$ is a unit vector in the direction joining second-nearest-neighbor sites i to j, and C is a coefficient quantifying such an interaction. We choose a value of C equal to 6.3×10^{-6} hartree/bohrμ_B^2 because it results [9] in the well-known spin cycloid of BFO bulk [7,17,18] that propagates along a $\langle 110 \rangle$ direction that is perpendicular to the direction of polarization. The effective Hamiltonian is used inside molecular dynamics simulations that solve the following equations of motion:

$$M_X \frac{d^2X}{dt^2} = -\frac{\partial E_{\text{tot}}}{\partial X},$$
$$\frac{d\mathbf{m}_i}{dt} = -\gamma \mathbf{m}_i \times [\mathbf{B}^i_{\text{eff}}(t) + \mathbf{h}^i(t)] - \gamma \frac{\lambda}{|\mathbf{m}_i|(1+\lambda^2)} \mathbf{m}_i \times (\mathbf{m}_i \times [\mathbf{B}^i_{\text{eff}}(t) + \mathbf{h}^i(t)]), \tag{3}$$

where, in the first equation, X is any (Voigt or Cartesian) component of the strain, local modes, and oxygen octahedral tiltings, and M_X represents the mass or moment of inertia associated with these degrees of freedom. This first equation therefore combines the effective Hamiltonian scheme with the conventional molecular dynamics simulations with variables η, $\mathbf{u}_i$, and $\boldsymbol{\omega}_i$. The second equation is the stochastic Landau-Lifshitz-Gilbert (LLG) equation [19,20]. There, the effective magnetic field $\mathbf{B}^i_{\text{eff}}$ acting on the magnetic dipole centered on the Fe site i is given by $\mathbf{B}^i_{\text{eff}} = -(\partial E_{\text{tot}}/\partial \mathbf{m}_i)$. γ is the gyromagnetic ratio, and λ is the Gilbert damping constant that is chosen here to be $\lambda = 10^{-4}$. This particular choice for the damping constant is done because it was found to satisfactorily reproduce properties of BFO bulk [21]. $\mathbf{h}^i(t)$ is a fluctuating field that allows us to mimic finite-temperature effects. The Cartesian components of $\mathbf{h}^i(t)$ are associated with white noise processes represented by $\langle \mathbf{h}^i \rangle = 0$, and $\langle \mathbf{h}^i_\alpha(t) \mathbf{h}^i_\beta(0) \rangle = 2(\lambda k_B T/\gamma |\mathbf{m}_i|)\delta_{\alpha,\beta}\delta(t)$, where α and β are Cartesian components, $\delta(t)$ is the delta function, and $\delta_{\alpha,\beta}$ is the Kronecker delta.

We use an $18 \times 18 \times 18$ supercell (29160 atoms) that is periodic along the x, y, and z axes—that are lying along the pseudocubic [100], [010], and [001] directions, respectively. The dynamics are performed at 5 K using NPT ensembles. The time step for the molecular dynamics simulation is 0.5 fs. As consistent with experiments [18,22–24], the simulations predict an $R3c$ ground state that is characterized by a polarization lying along the pseudocubic [111] direction and an antiphase-oxygen-octahedral-tilting vector $\langle \boldsymbol{\omega} \rangle_R$ lying along this same [111] direction [note that $\langle \boldsymbol{\omega} \rangle_R$ is defined as $(1/N)\sum_i \boldsymbol{\omega}_i (-1)^{n_x(i)+n_y(i)+n_z(i)}$, where $n_x(i)$, $n_y(i)$, and $n_z(i)$ are the integers locating the site i, and N is the number of Fe sites inside the supercell]. The predicted magnetic ground state is also found to be consistent with measurements on BFO bulk [7,17,18,25,26], since it is a spin cycloid propagating along the pseudocubic $[\bar{1}01]$ direction and for which third-nearest neighbors along the [111] polarization direction are aligned in an antiferromagnetic fashion. Such magnetic organization gives rise to a magnetic chirality vector (1) that is defined as $\boldsymbol{\kappa} = (1/N_p)\sum_{i,j} \mathbf{m}_i \times \mathbf{m}_j$, where $\mathbf{m}_i$ and $\mathbf{m}_j$ are two neighboring spins along the propagation direction of the cycloid and N_p is the number of such pairs, and (2) that lies along the pseudocubic $[1\bar{2}1]$ direction.

We now apply an electric field along the $[\bar{1}\,\bar{1}\,\bar{1}]$ direction (that is opposite to the initial electrical polarization) and for which each Cartesian component has a magnitude of 7×10^8 V/m. Note that such a field has the same order of magnitude as the one recently experimentally applied in BFO films, that is, 10^9 V/m [27]. Let us first concentrate on the time evolution of the structural properties under this field. Figure 1(a) shows the supercell average of the Cartesian components of the local modes ($\langle u_x \rangle$,$\langle u_y \rangle$,$\langle u_z \rangle$) as a function of time, while Fig. 1(b) displays similar data but for the $\langle \boldsymbol{\omega} \rangle_R$ antiferrodistortive vector. Figure 1(a) indicates that the electrical polarization first rapidly shrinks in magnitude with time, while still lying along [111], and then vanishes at a time $\simeq$200 fs. Increasing further the time above this critical value leads to a polarization now lying along the $[\bar{1}\,\bar{1}\,\bar{1}]$ direction (i.e., parallel to the applied electric field) that increases in magnitude until reaching a stable value for time at and above $\simeq$300 fs. In other words, Fig. 1(a) reveals an ultrafast switching of polarization which is very much desired in ferroelectric capacitors used in devices such as ferroelectric random access memory (or for multistate storage devices [28,29]) in order to write data

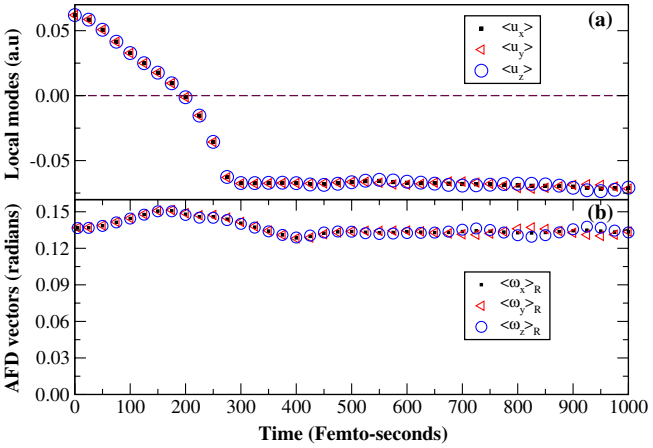

FIG. 1 (color online). Time evolution of (a) the supercell average of the local modes and of (b) the antiferrodistortive vector in BFO bulks under a dc electric field oriented along the $[\bar{1}\,\bar{1}\,\bar{1}]$ pseudocubic direction.

at a very fast scale. We also numerically found (by, e.g., performing Fourier transforms of the local modes [30]) that the predicted polarization switching is continuous, as similar to the case of $PbTiO_3$ films [31]. In other words, it does not involve domain nucleation and movement [32].

Interestingly, Fig. 1(b) reveals that any Cartesian component of $\langle \boldsymbol{\omega} \rangle_R$ first increases with time until reaching a maximum for times about which the polarization is the smallest in magnitude, and then decreases until slightly oscillating around a fixed value when further increasing the time. The opposite behavior of the magnitude of the polarization and oxygen octahedral tilting from 0 to $\simeq$300 fs reflects the well-known competitive behavior of these two structural degrees of freedom [10,33–38]. Moreover and unlike the polarization, $\langle \boldsymbol{\omega} \rangle_R$ does not switch in direction and thus remains oriented along the [111] direction at any time. Such lack of change of direction of $\langle \boldsymbol{\omega} \rangle_R$, even when the polarization is reversed, originates from the fact that the coupling between oxygen octahedral tilting and polarization is quadratic in both the AFD and FE degrees of freedom [10,39]. Figures 1(a) and 1(b) therefore reveal that the ultrafast switching of the polarization follows a path starting from one $R3c$ state (for which the polarization and $\langle \boldsymbol{\omega} \rangle_R$ are both along the pseudocubic [111] direction) and ending in another $R3c$ state (for which the polarization is now along $[\bar{1}\,\bar{1}\,\bar{1}]$ while the oxygen octahedral still tilts about [111]) via an $R\bar{3}c$ state that is characterized by a vanishing polarization and an enhanced $\langle \boldsymbol{\omega} \rangle_R$ that remains oriented along [111]. As demonstrated and detailed in the Supplemental Material [40], the coupling between polarization and oxygen octahedral tilting in BFO (and its effect on the coercive field [41]) provides a natural explanation for the ultrafast and homogeneous nature of the switching of the polarization, since this latter follows a path that is well defined by its strong coupling with the oxygen octahedral tilting. Note that this $R3c \rightarrow R\bar{3}c \rightarrow R3c$ path requires the application of an electric field along a $\langle 111 \rangle$ direction, unlike what is typically done in most experiments—for which the electric field lies along a $\langle 001 \rangle$ direction (see, e.g., Ref. [41] and references therein).

Let us now concentrate on the consequence of the switching of the polarization on magnetic properties. For that, Figs. 2(a) and 2(b) display the time evolution of the magnetic chirality vector and of the magnitude of the G-type antiferromagnetic (AFM) vector. This latter vector is denoted as $\langle \mathbf{L} \rangle_G$ and is given by $\langle \mathbf{L} \rangle_G = (1/N)\sum_i (-1)^{n_x(i)+n_y(i)+n_z(i)} \mathbf{m}_i$. Moreover, Figs. 3(a)–3(e) provide snapshots of the magnetic configuration along a given $[\bar{1}01]$ line joining Fe ions that are second-nearest neighbors of each other for five different specific times, respectively. Figures 2 and 3 reveal a quite complex and interesting electric-field-driven sequence of magnetic reorganization inside BFO bulk. For instance, during the time interval ranging between 0 and $\simeq$200 fs for which the polarization shrinks in magnitude along the pseudocubic

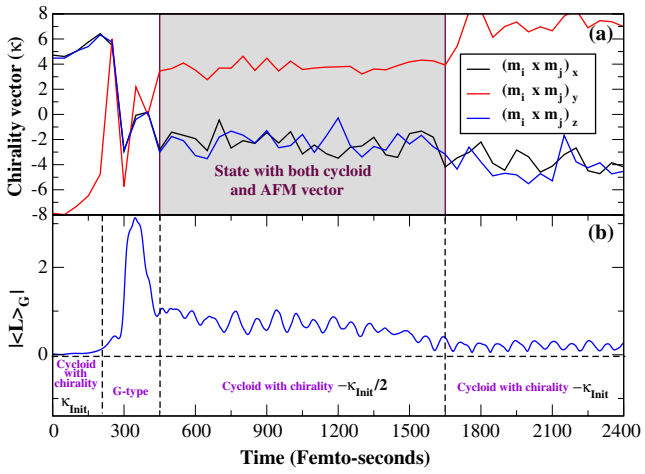

FIG. 2 (color online). Same as Fig. 1 but for (a) the magnetic chirality vector and (b) the magnitude of the G-type AFM vector.

[111] direction, the magnetic chirality vector remains merely unchanged. This result indicates that the initial magnetic cycloid does not respond to this ultrafast change of the polarization, as confirmed by comparing Figs. 3(a) and 3(b) that correspond to the initial time and $t = 100$ fs, respectively. On the other hand, between $\simeq$200 and $\simeq$400 fs, $\boldsymbol{\kappa}$ oscillates a lot and can adopt rather small magnitude, while the G-type AFM vector gains some considerable strength. We interpret such evolution as indicating that the magnetic sublattice has "noticed," with a time delay, that the polarization can be quite small during the application of a reverse electric field, and therefore the spin cycloid tends to be destroyed in favor of an intermediate state possessing a significant G-type AFM character—as consistent with the fact that the term $C(\mathbf{u}_i \times \mathbf{e}_{ij})$ in front of $\mathbf{m}_i \times \mathbf{m}_j$ in Eq. (2) is now small. Such a tendency is confirmed by looking at Fig. 3(c) that shows the organization of the magnetic dipoles at $t = 350$ fs: one can see that adjacent (second-nearest-neighbor) dipoles are rather parallel to each other, as expected

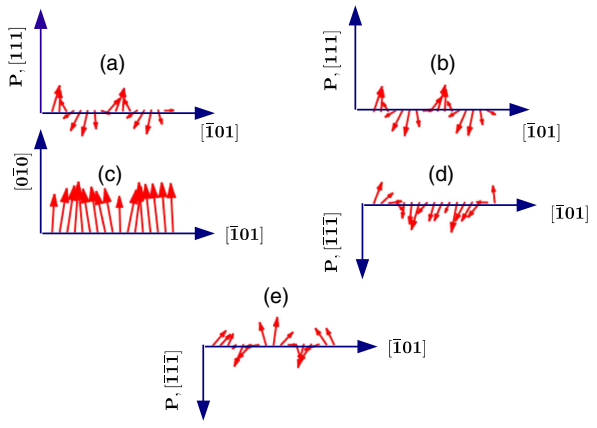

FIG. 3 (color online). Magnetic dipolar configurations along a specific $[\bar{1}01]$ line joining Fe ions for some specific times. (a)–(e) Times of 0, 100, 350, 1000, and 3000 fs, respectively.

in a G-type AFM structure. Note that we numerically found that the G-type AFM vector can rotate when time varies between ≃200 and ≃400 fs; e.g., it can lie along the [101], [0$\bar{1}$0], or [$\bar{1}$ $\bar{1}$ $\bar{1}$] pseudocubic direction. Moreover, for times comprised between 400 and 1650 fs (i.e., 1.65 ps), the magnetic chirality vector is quite stable with an intermediate value of $\boldsymbol{\kappa} \simeq -2\mathbf{x} + 4\mathbf{y} - 2\mathbf{z}$ (that is equal to $-(\boldsymbol{\kappa}_{\text{init}}/2)$, $\boldsymbol{\kappa}_{\text{init}}$ being the initial chirality of the cycloid) and the strength of $\langle \mathbf{L} \rangle_G$ has now decreased to a value ranging between $0.5\mu B$ and $1\mu B$. Such features indicate that the resulting magnetic configuration is another intermediate state that is characterized by the coexistence of a significant G-type antiferromagnetism altogether with a magnetic cycloid that occurs within the same plane as the initial magnetic cycloid but with a chirality opposite to the initial one. Figure 3(d) provides a snapshot of such magnetic reorganization for $t = 1000$ fs. Interestingly, we numerically found that this peculiar intermediate magnetic state owes its existence to a combination of magnetic damping and magnitude of the electric field. More precisely and as shown in the Supplemental Material [42], decreasing the value of the damping coefficient for the presently selected magnitude of the electric field tends to shrink the time window for which this magnetic intermediate state can occur. This is because the magnetic degrees of freedom can more easily follow the effective magnetic field resulting from the energy of Eq. (2), when damping is smaller. On the other hand, decreasing the magnitude of the electric field for our presently selected and realistic value of the damping coefficient results in a smaller magnitude of the local modes and thus leads to a smaller effective magnetic field. As a result, the magnetic degrees of freedom experience more problems to follow the dynamics of the local modes and thus spend more time in this intermediate magnetic state. Finally, for times above 1650 fs and as shown in Fig. 3(e), the G-type AFM vector is nearly annihilated and the magnetic arrangement now consists of a spin cycloid that has a chirality vector that is exactly opposite to the initial one [as consistent with the analytical form of Eq. (2) that indicates that reversing the electrical polarization should revert the cross products between the $\mathbf{m}_i$ and $\mathbf{m}_j$ vectors]. In other words, the complete switching of the magnetic chirality has occurred around 1.65 ps and has therefore taken around 6 times longer than the switching of the polarization but is still ultrafast in nature. Such ultrafast switching of the chiral state is very promising and much more advantageous compared to devices where switching of the magnetic state is achieved by injecting current, since the latter process generates much more Joule heating. Moreover, the presently discovered electric-field-driven magnetic switching has involved quite a complex sequence of magnetic arrangements, which can, in fact, be taken as an advantage over systems exhibiting both a polarization ($\mathbf{P}$) and a magnetization ($\mathbf{M}$). As a matter of fact, while these latter systems can, in theory, exhibit four different states—namely, ($\mathbf{P}$, $\mathbf{M}$), ($-\mathbf{P}$, $\mathbf{M}$), ($\mathbf{P}$, $-\mathbf{M}$), and ($-\mathbf{P}$, $-\mathbf{M}$)—only two of them are easily accessible [43] due to large magnetoelectric couplings [28]. Here, in contrast, three different well-defined states can be easily accessed when applying a field along [$\bar{1}$ $\bar{1}$ $\bar{1}$]. They are ($\mathbf{P}$, $\boldsymbol{\kappa}_{\text{init}}$) for time ranging between 0 and 200 fs, ($-\mathbf{P}$, $-(\boldsymbol{\kappa}_{\text{init}}/2)$) for t being in between 400 and 1650 fs, and ($-\mathbf{P}$, $-\boldsymbol{\kappa}_{\text{init}}$) for times above. Interestingly, applying then a field along [111] from the final ($-\mathbf{P}$, $-\boldsymbol{\kappa}_{\text{init}}$) state was also numerically found (not shown here) to lead to the situation in which the polarization and magnetic chiralities are precisely reversed with respect to the case indicated in Figs. 1–3. As a result, a fourth state appears, which is a mixed state characterized by ($\mathbf{P}$, $\boldsymbol{\kappa}_{\text{init}}/2$), therefore rendering the possibility of making a four-state memory device possible [28,29] (see the schematization in Fig. 4). Such memories could have all the combined advantages of ferroelectric random access memory [44] and magnetic random access memory [45]. For instance, one would be able to write the data using very low power (as in ferroelectric random access memory) and read data in a nondestructive way (as in magnetic random access memory, since magnetic switching does not require any movement of ions). Note that changes in magnetic chirality may be practically observed via Kerr, Hall, or optical effects [46,47].

Note that we chose to report here properties at 5 K in order to get better statistics (i.e., less noise) for physical properties, especially those related to magnetism. However, we also numerically found that results similar to those depicted here can systematically occur at room temperature, especially if one uses slightly larger electric fields (to overcome the temperature-induced fluctuation of the electric dipoles) and a slightly smaller damping constant (to allow the magnetic degrees of freedom to more easily follow the coupled polarization dynamics).

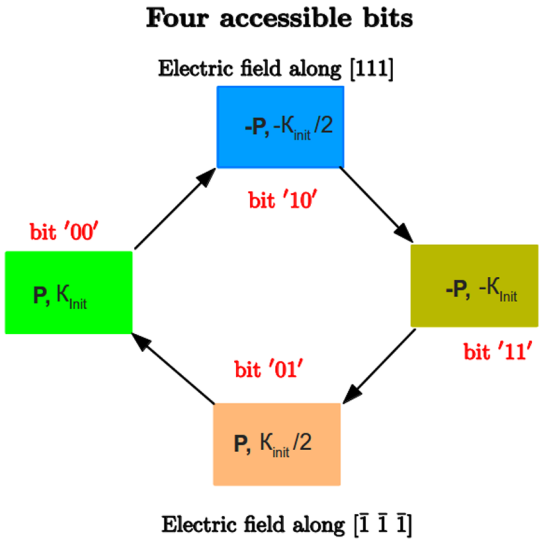

FIG. 4 (color online). Schematization of the proposed four-state memory.

We hope that our study deepens the knowledge of multiferroics and will encourage investigations aimed at confirming and exploiting our results.

We are grateful to M. Bibes for stimulating discussions. We acknowledge ARO Grant No. W911NF-12-1-0085 (S. B. and L. B.) for running and analyzing the simulations, and NSF Grant No. DMR-1066158 (D. R. and L. B.) for determining the energy associated with the magnetic cycloid and investigating electric field effects in multiferroics. The Office of Basic Energy Sciences, under Contract No. ER-46612, and ONR Grants No. N00014-11-1-0384 and No. N00014-12-1-1034 are also acknowledged for discussions with scientists sponsored by these grants. J. I. had financial support from MINECO-Spain (Grants No. MAT2010-18113 and No. CSD2007-00041).

*sbhattac@uark.edu

[1] C. Pappas, Physics **5**, 28 (2012).
[2] R. Antos and Y. Otani, Phys. Rev. B **80**, 140404(R) (2009).
[3] M. Bode, M. Heide, K. von Bergmann, P. Ferriani, S. Heinze, G. Bihlmayer, A. Kubetzka, O. Pietzsch, S. Blügel, and R. Wiesendanger, Nature (London) **447**, 190 (2007).
[4] S. Onoda and N. Nagaosa, Phys. Rev. Lett. **90**, 196602 (2003).
[5] A. Fert, Mater. Sci. Forum **59–60**, 439 (1990).
[6] T. Zhao *et al.*, Nat. Mater. **5**, 823 (2006).
[7] D. Lebeugle, D. Colson, A. Forget, M. Viret, A. M. Bataille, and A. Gukasov, Phys. Rev. Lett. **100**, 227602 (2008).
[8] S. Lee, T. Choi, W. Ratcliff, R. Erwin, S.-W. Cheong, and V. Kiryukhin, Phys. Rev. B **78**, 100101 (2008).
[9] D. Rahmedov, D. Wang, J. Iniguez, and L. Bellaiche, Phys. Rev. Lett. **109**, 037207 (2012).
[10] I. A. Kornev, L. Bellaiche, P. E. Janolin, B. Dkhil, and E. Suard, Phys. Rev. Lett. **97**, 157601 (2006).
[11] J. B. Neaton, C. Ederer, U. V. Waghmare, N. A. Spaldin, and K. M. Rabe, Phys. Rev. B **71**, 014113 (2005).
[12] W. Zhong, D. Vanderbilt, and K. M. Rabe, Phys. Rev. B **52**, 6301 (1995).
[13] I. A. Kornev, S. Lisenkov, R. Haumont, B. Dkhil, and L. Bellaiche, Phys. Rev. Lett. **99**, 227602 (2007).
[14] D. Albrecht, S. Lisenkov, W. Ren, D. Rahmedov, I. A. Kornev, and L. Bellaiche, Phys. Rev. B **81**, 140401 (R) (2010).
[15] H. Katsura, N. Nagaosa, and A. V. Balatsky, Phys. Rev. Lett. **95**, 057205 (2005).
[16] A. Raeliarijaona, S. Singh, H. Fu, and L. Bellaiche, Phys. Rev. Lett. **110**, 137205 (2013).
[17] I. Sosnowska, M. Loewenhaupt, W. I. F. David, and R. M. Ibberson, Physica (Amsterdam) **180B–181B**, 117 (1992).
[18] I. Sosnowska, T. Peterlin-Neumaier, and E. Steichele, J. Phys. C **15**, 4835 (1982).
[19] L. Landau and E. Lifshitz, Phys. Z. Sowjetunion **8**, 153 (1935).
[20] T. L. Gilbert, IEEE Trans. Magn. **40**, 3443 (2004).
[21] D. Wang, J. Weerasinghe, and L. Bellaiche, Phys. Rev. Lett. **109**, 067203 (2012).
[22] F. Kubel and H. Schmid, Acta Crystallogr. Sect. B **46**, 698 (1990).
[23] J. D. Bucci, B. K. Robertson, and W. J. James, J. Appl. Crystallogr. **5**, 187 (1972).
[24] J. R. Teague, R. Gerson, and W. J. James, Solid State Commun. **8**, 1073 (1970).
[25] J. Jeong *et al.*, Phys. Rev. Lett. **108**, 077202 (2012).
[26] M. Ramazanoglu, M. Laver, W. Ratcliff, S. M. Watson, W. C. Chen, A. Jackson, K. Kothapalli, S. Lee, S.-W. Cheong, and V. Kiryukhin, Phys. Rev. Lett. **107**, 207206 (2011).
[27] H. Yamada *et al.*, ACS Nano **7**, 5385 (2013).
[28] J. F. Scott, Nat. Mater. **6**, 256 (2007).
[29] M. Bibes and A. Barthelemy, Nat. Mater. **7**, 425 (2008).
[30] A. M. George, J. Íñiguez, and L. Bellaiche, Phys. Rev. B **65**, 180301(R) (2002).
[31] M. J. Highland, T. T. Fister, M.-I. Richard, D. D. Fong, P. H. Fuoss, C. Thompson, J. A. Eastman, S. K. Streiffer, and G. Brian Stephenson, Phys. Rev. Lett. **105**, 167601 (2010).
[32] G. B. Stephenson and M. J. Highland, Phys. Rev. B **84**, 064107 (2011).
[33] L. Bellaiche and J. Iñiguez, Phys. Rev. B **88**, 014104 (2013).
[34] D. Vanderbilt and W. Zhong, Ferroelectrics **206**, 181 (1998).
[35] J. C. Wojdel, P. Hermet, M. P. Ljungberg, P. Ghosez, and J. Iñiguez, J. Phys. Condens. Matter **25**, 305401 (2013).
[36] I. C. Infante *et al.*, Phys. Rev. Lett. **105**, 057601 (2010).
[37] D. Sichuga and L. Bellaiche, Phys. Rev. Lett. **106**, 196102 (2011).
[38] B. Houchmandzadeh, J. Lajzerowicz, and E. Salje, J. Phys. Condens. Matter **3**, 5163 (1991).
[39] I. A. Kornev and L. Bellaiche, Phys. Rev. B **79**, 100105(R) (2009).
[40] See Supplemental Material at http://link.aps.org/supplemental/10.1103/PhysRevLett.112.147601 which includes Refs. [13,30,39,43].
[41] P. Maksymovych *et al.*, Phys. Rev. B **85**, 014119 (2012).
[42] R. Kikuchi, J. Appl. Phys. **27**, 1352 (1956).
[43] M. Gajek, M. Bibes, S. Fusil, K. Bouzehouane, J. Fontcuberta, A. Barthélémy, and A. Fert, Nat. Mater. **6**, 296 (2007).
[44] H. Ishiwara, J. Nanosci. Nanotechnol. **12**, 7619 (2012).
[45] J. Akerman, Science **308**, 508 (2005).
[46] S. R. Bowden, K. K. Ahmed, and U. J. Gibson, Appl. Phys. Lett. **91**, 232505 (2007).
[47] A. Demiray, M. Kohda, and J. Nitta, Appl. Phys. Lett. **103**, 122408 (2013).